

Fat Fisher Zeroes

W. Janke

Institut für Theoretische Physik
Universität Leipzig
D-04109 Leipzig
Germany

and

D.A. Johnston and M. Stathakopoulos

Dept. of Mathematics
Heriot-Watt University
Riccarton
Edinburgh, EH14 4AS, Scotland

November 3, 2018

Abstract

We show that it is possible to determine the locus of Fisher zeroes in the thermodynamic limit for the Ising model on planar (“fat”) ϕ^4 random graphs and their dual quadrangulations by matching up the real part of the high and low temperature branches of the expression for the free energy. The form of this expression for the free energy also means that series expansion results for the zeroes may be obtained with rather less effort than might appear necessary at first sight by simply reverting the series expansion of a function $g(z)$ which appears in the solution and taking a logarithm.

Unlike regular 2D lattices where numerous unphysical critical points exist with non-standard exponents, the Ising model on planar ϕ^4 graphs displays only the physical transition at $c = \exp(-2\beta) = 1/4$ and a mirror transition at $c = -1/4$ both with KPZ/DDK exponents ($\alpha = -1, \beta = 1/2, \gamma = 2$). The relation between the ϕ^4 locus and that of the dual quadrangulations is akin to that between the (regular) triangular and honeycomb lattices since there is no self-duality.

1 Introduction

One of the more remarkable results to emerge from the study of various statistical mechanical models coupled to two-dimensional quantum gravity is a solution of the Ising model in field [1, 2]. In discrete form the coupling to gravity takes the form of the spin models living on an annealed ensemble of triangulations or quadrangulations, or their dual planar graphs. The partition function for the Ising model on a single graph G^n with n vertices

$$Z_{\text{single}}(G^n, \beta, h) = \sum_{\{\sigma\}} e^{\beta \sum_{\langle i, j \rangle} \sigma_i \sigma_j + h \sum_i \sigma_i}, \quad (1)$$

is promoted to a partition function which incorporates a sum over some class of graphs $\{G^n\}$ by the coupling to gravity

$$Z_n(\beta, h) = \sum_{\{G^n\}} Z_{\text{single}}(G^n, \beta, h). \quad (2)$$

That introducing such an annealed sum over graphs into the partition function should be a discrete version of coupling to gravity becomes clearer when one considers the approach taken to simulating such models. In simulations one changes both the geometry (i.e. connectivity) of the lattice and the spins on the same timescale, so the spins affect the geometry and vice-versa, mimicking the back-reaction of matter and gravitation in the continuum theory. The solution to the Ising model in [1] proceeded by first forming the grand canonical partition function

$$\mathcal{Z} = \sum_{n=1}^{\infty} \left(\frac{-4gc}{(1-c^2)^2} \right)^n Z_n(\beta, h) \quad (3)$$

and then noting that this could be expressed as the free energy

$$\mathcal{Z} = -\log \int \mathcal{D}\phi_1 \mathcal{D}\phi_2 \exp \left(-\text{Tr} \left[\frac{1}{2}(\phi_1^2 + \phi_2^2) - c\phi_1\phi_2 - \frac{g}{4}(e^h\phi_1^4 + e^{-h}\phi_2^4) \right] \right) \quad (4)$$

of a matrix model, where we have written the potential that generates ϕ^4 graphs. In the above $\phi_{1,2}$ are $N \times N$ Hermitian matrices, $c = \exp(-2\beta)$ and the $N \rightarrow \infty$ limit is performed in order to pick out planar graphs. The graphs of interest are generated as the Feynman diagrams of the “action” in equ.(4), which is constructed so as to weight each edge with the correct Boltzmann weights for nearest neighbour interaction Ising spins. Since the edges carry matrix indices the graphs in question are “fat” or ribbon graphs.

The integral of equ.(4) can be evaluated using the results of [3] to give

$$\mathcal{Z} = \frac{1}{2} \log \left(\frac{z}{g} \right) - \frac{1}{g} \int_0^z \frac{dt}{t} g(t) + \frac{1}{2g^2} \int_0^z \frac{dt}{t} g(t)^2, \quad (5)$$

where g is defined by

$$g(z) = 3c^2 z^3 + z \left[\frac{1}{(1-3z)^2} - c^2 + \frac{6z(\cosh h - 1)}{(1-9z^2)^2} \right]. \quad (6)$$

The implicit form of the solution may make it a little difficult to see what is going on, but since the singularities of \mathcal{Z} w.r.t. g determine the asymptotics of the Z_n , the procedure for extracting the thermodynamic limit is to look at the solutions to $g'(z) = 0$. These can be explicitly determined when $h = 0$ as $z_L = -1/3$, $z_{H_{1,2}} = (1/3)[1 \mp \frac{1}{\sqrt{c}}]$, $z_{H_{3,4}} = (1/3)[1 \pm \frac{1}{\sqrt{-c}}]$ and then substituted into g

$$\begin{aligned} g_L(c) &= -\frac{1}{12} + \frac{2}{9}c^2, \\ g_{H_{1,2}}(c) &= \frac{2}{3}c - \frac{2}{9}c^2 \mp \frac{4}{9}\sqrt{c}, \\ g_{H_{3,4}}(c) &= -\frac{2}{3}c - \frac{2}{9}c^2 \mp \frac{4}{9}\sqrt{-c}, \end{aligned} \quad (7)$$

where z_L is the low-temperature branch and the various z_H high-temperature branches. Inserting the appropriate $g(c)$ into the expression for Z_n

$$Z_n \sim n^{-b} \left[\frac{-4cg(c)}{(1-c^2)^2} \right]^{-n} \quad (8)$$

then gives the asymptotics of the Z_n and the thermodynamic behaviour of the free energy per site F

$$F = -\log \left[\frac{-4cg(c)}{(1-c^2)^2} \right], \quad (9)$$

since if we are given a canonical partition function Z_n the associated free energy per site F will be given in the thermodynamic limit by

$$F \sim \lim_{n \rightarrow \infty} \frac{1}{n} \log Z_n. \quad (10)$$

The third order phase transition with the so-called KPZ/DDK [4] exponents, $\alpha = -1$, $\beta = 1/2$, $\gamma = 2$ occurs when $g_L(c) = g_{H_1}(c)$ which gives a critical coupling $c = 1/4$. It is possible to carry out a perturbative expansion in h around the $h = 0$ solutions above to obtain the magnetic critical exponents directly from the discretized formulation [2] and it is likewise possible to confirm universality by solving the model on ϕ^3 graphs. The KPZ/DDK exponents were verified in a continuum formalism in [4] using conformal field theory techniques.

Given the solution of [1, 2] it is tempting to use it as a test case to investigate various statistical mechanical ideas and methods, in much the same manner as the Onsager solution has served as a paradigm over many years. One such effort was presented in [5], where the behaviour of the partition function zeroes for the Ising model coupled to two-dimensional quantum gravity was investigated by series expansion and numerical means. The study of partition function zeroes for statistical mechanical models was initiated by Lee and Yang for complex external fields [6, 7] and later extended by Fisher and others to complex temperatures [8]. It offers an alternative viewpoint of the approach to the thermodynamic limit and means of extracting critical exponents. A study of partition function zeroes for the Ising model coupled to two-dimensional gravity addresses several interesting questions. It is not clear *a priori* that loci of partition function zeroes will continue to lie on simple curves in the $c = \exp(-2\beta)$ or $y = \exp(-2h)$ planes when a sum over some class of graphs, in this case planar graphs, is folded into the partition function. Although this is generically the case for the Onsager and related solutions on regular two-dimensional lattices [9, 10], there are exceptions such as the “bathroom-tile” lattice. Other sorts of behaviour are possible too. For instance, introducing geometric disorder in the form of Penrose tilings gave an complicated extended structure of temperature zeroes away from the physical critical point, but still gives rise to Onsager exponents [11]. Fractal lattices on the other hand display an intricate fractal pattern of zeroes [12].

The work in [5] suggested strongly that the temperature zeroes *did* lie on curves and that the field zeroes still lay on the unit circle in the complex $y = \exp(-2h)$ plane, as in the regular lattice Onsager solution. Similarly, a comprehensive analytical study of the Lee-Yang zeroes for the Ising model on planar ϕ^4 graphs was carried out in [13], where it was found implicitly that the Lee-Yang circle theorem still held, since the complex field singularities were shown to lie at purely imaginary field values. In this paper we concentrate on the temperature (Fisher) zeroes for the Ising model on planar ϕ^4 graphs and their dual quadrangulations, showing how to derive the locus of zeroes analytically using the idea that the locus should be thought of as Stokes lines [9, 10, 12, 14, 15]. We compare the results with the various sorts of behaviour observed in [9, 10] for regular two-dimensional lattices and also note that the form of the Ising solution means that the various zeroes on finite planar ϕ^4 graphs can be extracted without evaluating a series expansion for the full expression for \mathcal{Z} . In the sequel we first briefly discuss the general background to Lee-Yang and Fisher zeroes and the analytic determination of the loci of zeroes. We then show how series expansion results for finite graphs, such as those in [5], can be recovered and extended economically before we move on to discuss obtaining the loci of Fisher zeroes for the Ising model on ϕ^4 graphs and their duals analytically.

2 Lee-Yang and Fisher Zeroes

The starting point of Lee and Yang's work [6, 7] was the consideration of how the non-analyticity characteristic of a phase transition appeared from the partition function on finite lattices or graphs, which was a polynomial

$$Z = \sum D_{mn} c^m y^n \quad (11)$$

for a lattice with m edges and n vertices, again with $c = \exp(-2\beta)$, $y = \exp(-2h)$. They showed that the behaviour of the zeroes of this polynomial in the complex z plane, in particular the limiting locus as $m, n \rightarrow \infty$, determined the phase structure. Similarly, the behaviour of the zeroes in the complex c plane determines the nature of temperature driven transitions [8]. In the latter case, in zero external field for simplicity, the free energy on some lattice or graph G_n with n nodes and m edges can be written

$$F(G_n, \beta) \sim -\ln \prod_{k=1}^m (c - c_k(\beta)), \quad (12)$$

which in the thermodynamic limit becomes

$$F(G_\infty, \beta) \sim - \int_L dc \rho(c) \ln(c - c(L)), \quad (13)$$

where L is some set of curves, or possibly regions, in the complex c plane on which the zeroes have support and $\rho(c)$ is the density of the zeroes there. The singular behaviour of $\rho(c)$ as c approaches the physical transition point c_{PT} is related to the specific heat exponent α by

$$\rho(c) \sim (c - c_{PT})^{1-\alpha}. \quad (14)$$

The general question of how to extract the locus of zeroes analytically has been considered by various authors. It was observed in [12] that such loci could be thought of as Stokes lines separating different regions of asymptotic behaviour of the partition function in the complex temperature or field planes. Across these lines the real part of the free energy should be continuous and the discontinuity in the imaginary part should give the density of zeroes. Shrock and collaborators [9, 10, 14] have obtained many interesting and explicit results on the Fisher and Lee-Yang loci for the Ising and other models on regular lattices by matching free energies in this manner. They also observed that the condition $\Re \xi^{-1} = 0$, where ξ was the correlation length, gave equivalent loci [14]. Both this condition and the matching of free energies are consistent with the idea that the loci of zeroes coincide with a change of dominant behaviour in the asymptotics.

More recently, the case of models with first-order transitions has been investigated by Biskup *et al.* [15] who showed rigorously ¹ that the partition function of a d -dimensional statistical mechanical model defined in a periodic volume $V = L^d$ which depends on some complex parameter such as c or y can be written in terms of complex functions F_l describing k different phases as

$$Z = \sum_l^k q_l e^{-\beta F_l V} + O(e^{-L/L_0} e^{-\beta F V}), \quad (15)$$

where q_l is the degeneracy of phase l , β is the inverse temperature and L_0 is of the order of the correlation length. The various F_l are the metastable free energies per unit volume of the phases, with $\Re F_l = F$ characterising the free energy when phase l is stable. The zeroes of the partition function are then determined to lie within $O(e^{-L/L_0})$ of the solutions of the equations

$$\begin{aligned} \Re F_{l,L}^{eff} &= \Re F_{m,L}^{eff} < \Re F_{k,L}^{eff}, \quad \forall k \neq l, m, \\ \beta V (\Im F_{l,L} - \Im F_{m,L}) &= \pi \bmod 2\pi. \end{aligned} \quad (16)$$

¹Under suitable technical conditions.

The equations (16) are thus in perfect agreement with the idea that the loci of zeroes should be Stokes lines, since the zeroes of Z asymptotically lie on the complex phase coexistence curves $\Re F_{l,L} = \Re F_{m,L}$ in the complex parameter plane.

The specific Biskup *et al.* results apply to models with first order transitions – the canonical example being the field-driven transition for the Ising model, and we are interested here in a model with a third order transition, so it might initially seem that these results were inapplicable. We are saved by the fact that when considered in the complex temperature plane the transition is continuous only at the physical point itself (and possibly some other finite set of points). This is nicely illustrated by looking at expressions for the magnetization for the Ising model on the square lattice, on fat (planar) ϕ^4 graphs and on thin (generic) ϕ^3 graphs:

$$\begin{aligned} M &= \frac{(1+u)^{1/4}(1-6u+u^2)^{1/8}}{(1-u)^{1/2}} \quad (\text{square}), \\ M &= \frac{3(1-16u)^{1/2}}{3-8u} \quad (\text{fat } \phi^4), \\ M &= \frac{(1-3c)^{1/2}}{(1-2c)(1+c)^{1/2}} \quad (\text{thin } \phi^3), \end{aligned} \tag{17}$$

where $u = c^2 = \exp(-4\beta)$. It is clear from these expressions, which apply through the complex extension of the low-temperature phase with M zero outside, that although M will vanish continuously at the physical critical points, $u = 3 - 2\sqrt{2}$; $u = 1/16$ (i.e. $c = 1/4$); $c = 1/3$ respectively ², it will generally be non-zero at the phase boundary approaching from within the low-temperature region, whereas it will be zero approaching from outside, which is characteristic of a first-order transition.

In summary, both general considerations about the change of asymptotic behaviour of expansions of the partition function in different regions of the complex temperature or field planes [12, 14, 9, 10] and rigorous results [15] lead to equ.(16) as a means of determining the loci of zeroes.

3 Series Expansions With (two thirds) Less Pain

To get a series expansion for \mathcal{Z} one must in principle go back to equ.(5) and invert (or more correctly, revert) the expression for $g(z)$ in equ.(6) expanded as a series in z to get an expansion $z(g)$ in powers of g . This is then inserted in equ.(5) in order to obtain the desired series from which the zeroes may be extracted. However, if one considers the various terms in equ.(5) independently some interesting observations can immediately be made. Taking each of the terms in equ.(5) separately,

$$\begin{aligned} \mathcal{Z}_1 &: \quad \frac{1}{2} \log \left(\frac{z}{g} \right), \\ \mathcal{Z}_2 &: \quad -\frac{1}{g} \int_0^z \frac{dt}{t} g(t), \\ \mathcal{Z}_3 &: \quad \frac{1}{2g^2} \int_0^z \frac{dt}{t} g(t)^2, \end{aligned} \tag{18}$$

the series expansion of each term $k = 1, 2, 3$ can be written as $\mathcal{Z}_k = \sum_n a_k^n A_n(c^2) g^n$ where $A_n(c^2)$ is *identical* for all the \mathcal{Z}_k . In addition, normalizing $a_n = 1$ for the $\frac{1}{2} \log \left(\frac{z}{g} \right)$ term (since any n dependence in this can be put in A_n), one finds

$$\begin{aligned} a_1^n &= 1, \\ a_2^n &= \frac{n}{(n+2)}, \end{aligned} \tag{19}$$

²There are further points where the magnetization vanishes continuously: at the anti-ferromagnetic point $u = 3 + 2\sqrt{2}$ and the unphysical point $u = -1$ on the square lattice; and the unphysical point $c = -1/4$ on the planar ϕ^4 graphs, but these are discrete and finite in number.

$$a_3^n = -\frac{2n}{(n+1)}.$$

Although the $A_n(c^2)$ which determine the partition function zeroes for a given power of g are the same for each \mathcal{Z}_k , this is obscured by the different a_k^n in the sum $\mathcal{Z}_1 + \mathcal{Z}_2 + \mathcal{Z}_3$.

Why should this structure be present? The solution given in equ.(5) comes from integrating an expression of the form

$$\mathcal{Z} = \int_0^1 dx (1-x) \log(f(x)) + \dots \quad (20)$$

which is common in form to all matrix models. The particular details of a given model are encoded in the $f(x)$ which for the Ising model with $h = 0$ satisfies

$$gx = \left(\frac{2gf}{c} \right) \left(\frac{1}{(1 - \frac{6gf}{c})^2} - c^2 \right) + 3c^2 \left(\frac{2gf}{c} \right)^3. \quad (21)$$

The expression in equ.(5) emerges on defining $z = \frac{2gf}{c}$ and integrating by parts.

If we expand the $\log(f(x))$ in the integrand of equ.(20), then we get $\int dx (1-x) P(gx, c)$, where $P(gx, c)$ is a power-series in gx . Looking at the structure of $P(gx, c)$ it is clear that the integration over x only affects numerical factors, but *not* the c^2 -polynomials which determine the zeroes. If we now carry out the partial integration on the $P(gx, c)$, we obtain three terms: $P(1, c)/2$ from the boundary corresponding to \mathcal{Z}_1 (and irrelevant additional terms); $-\int dx x P'(gx, c)$ corresponding to \mathcal{Z}_2 ; and $\frac{1}{2} \int dx x^2 P'(gx, c)$ corresponding to \mathcal{Z}_3 . Carrying out the differentiation of the power series $P'(gx, c)$, followed by the integration above recovers the observed values of the a_k^n .

The upshot of all of this is that for the purposes of extracting partition function zeroes it is sufficient to simply consider the expansion of $\log(z(g)/g)$ in powers of g , by reverting the series for $g(z)$,

$$g = (1 - c^2)z + 6z^2 + 3(c^2 + 9)z^3 + \dots, \quad (22)$$

to get

$$\tilde{z}(\tilde{g}) = \tilde{g} - 6\tilde{g}^2 + 3(c^2 + 5)(c^2 + 3)\tilde{g}^3 + \dots \quad (23)$$

and then taking $\log(\tilde{z}(\tilde{g})/\tilde{g})$, where we have rescaled $z \rightarrow (c^2 - 1)\tilde{z}$, $g \rightarrow (c^2 - 1)^2\tilde{g}$ for algebraic convenience. The polynomial in c^2 in front of the appropriate power of \tilde{g} will then yield the desired Fisher zeroes. Various efficient algorithms exist for the reversion of series (i.e. getting from equ.(22) to equ.(23) and we have used both the built in algorithms in Maple and Mathematica and one of the earliest numerical algorithms, Newton iteration, to revert the series for $g(z)$ [16], all with identical results.

For the Newton iteration when $h = 0$ we take our starting function to be

$$f = (c^2 - 1)\tilde{g}(3(c^2 - 1)\tilde{z} - 1)^2 - \tilde{z} + (c^2\tilde{z} - 3c^2(c^2 - 1)^2\tilde{z}^3)(3(c^2 - 1)\tilde{z} - 1)^2. \quad (24)$$

This is then iterated with the standard Newton formula [16]

$$\tilde{z}_{k+1} = \tilde{z}_k - \frac{f(\tilde{z}_k)}{f'(\tilde{z}_k)} \quad (25)$$

with the starting condition $\tilde{z}_0 = \tilde{g}$ (see equ.(23) above). Since Newton iteration displays quadratic convergence the iteration index k is related to the order of the expansion i for \tilde{z} in \tilde{g} by $i = 2^k$. We thus get order $2^k - 1$ for $\tilde{z}(\tilde{g})/\tilde{g}$ in k iterations. This is both an advantage and a disadvantage since, although long series are generated quite rapidly, they are doubling in length at each iteration which can rapidly exhaust the available memory. With the built in functions on the other hand, one can proceed incrementally in the order.

To verify that $\log(\tilde{z}(\tilde{g})/\tilde{g})$ really is sufficient to determine the zeroes correctly we can compare the results for the zeroes in c coming from the polynomial coefficient at a given order in the expansion of

$\log(\tilde{z}(\tilde{g})/\tilde{g})$, for instance \tilde{g}^{14} ,

$$\begin{aligned}
& \frac{84768120}{7}c^{28} + 5255623440c^{26} + 547079930820c^{24} \\
& + 17774272305360c^{22} + 256588440930000c^{20} + 1908495144456480c^{18} \\
& + 7988644803377340c^{16} + \frac{138652618561302240}{7}c^{14} + 30012882991193160c^{12} \\
& + 28216084061998800c^{10} + 16541610886750140c^8 + 6002231595716880c^6 \\
& + 1335148577661600c^4 + 173901100089600c^2 + \frac{95938227092700}{7}, \tag{26}
\end{aligned}$$

with the results from the full expression for \mathcal{Z} from [5].³ There is complete agreement between the numerical values of the zeroes obtained with either method as shown in Table 1,

17.26983082 <i>I</i>	9.620359803 <i>I</i>	4.237939134 <i>I</i>
3.307585457 <i>I</i>	2.153341531 <i>I</i>	1.952696297 <i>I</i>
$\pm.2259213695 + .3562012608I$	$\pm.1989588142 + .6083974700I$	$\pm.1697220421 + .9027390050I$
	$\pm.1285487771 + 1.322771774I$	

Table 1: The zeroes from an expansion of both $\log(\tilde{z}(\tilde{g})/\tilde{g})$ and \mathcal{Z} to order \tilde{g}^{14} are identical. The complex conjugates of all the values shown are also zeroes.

It is easy to obtain an expansion of $\log(\tilde{z}(\tilde{g})/\tilde{g})$ in \tilde{g} up to quite high order with relatively modest computing facilities. The coefficient of \tilde{g}^{79} from such an expansion is given in Appendix A and we use this for comparison with the analytical expressions for the loci of Fisher zeroes in the next section.

The observations above regarding the sufficiency of $\log(\tilde{z}(\tilde{g})/\tilde{g})$ for determining the partition function zeroes also apply to both Lee-Yang zeroes and the Fisher zeroes in non-zero field, since the general structure of the expression for $\mathcal{Z} = \int_0^1 dx(1-x)\log(f(x)) + \dots$ is unchanged when the field is turned on – it is the defining equation for $f(x)$ which is altered. A nice confirmation of this can be obtained by using the series expansion of $\log(\tilde{z}(\tilde{g})/\tilde{g})$ to obtain the field zeroes in the variable $y = \exp(-2h)$ which are plotted in Fig. 1 for an expansion up to $O(31)$ with $c = 1/4$. These clearly lie on the unit circle, as they do for the full partition function, and are also evenly distributed. Similarly, Fisher zeroes for the partition function in field can also be investigated by expanding $\log(\tilde{z}(\tilde{g})/\tilde{g})$, using the full expression in equ.(6) with $h \neq 0$. The flow observed reproduces that seen in [5] where the complete partition function was considered (at much lower order).

4 The Locus of Zeroes on ϕ^4 Graphs

The determination of the locus of Fisher zeroes in the thermodynamic limit turns out to be rather straightforward, as we now describe. Since we wish to match $\Re F$ between the various solution branches to obtain the loci of Fisher zeroes and from equ.(10) $F \sim \log(g(c))$, the equation which determines the loci of zeroes in the thermodynamic limit is

$$\log |g_L(c)| = \log |g_{H_i}(c)|, \tag{27}$$

or more concisely

$$|g_L(c)| = |g_{H_i}(c)| \tag{28}$$

where the various g are given in equ.(8) and $i = 1, 2, 3, 4$ where appropriate depending on the region of the complex c plane. The explicit expressions arising from substituting a complex value of c into equ.(28)

³We would like to thank the authors of [5] for providing us with their original data.

are not very illuminating and we do not reproduce them here, but they allow the resulting curves to be plotted with Maple or Mathematica.

For comparison it is useful to refer back to the locus of Fisher zeroes for the Ising model on a regular square lattice, which is the limaçon in the complex $u = c^2 = \exp(-4\beta)$ plane shown in Fig. 2. The use of u has the advantage of subsuming the $c \rightarrow -c$ symmetry that is present in the solution and is perhaps the most natural choice of variable. The (complex extended) ferromagnetic phase lies inside the inner loop, the paramagnetic phase between the loops and the antiferromagnetic phase in the exterior. The physical ferromagnetic and antiferromagnetic transition points lie on the positive real axis at $u = 3 \mp \sqrt{2}$ and a multiple point with non-standard exponents is present at $u = -1$, as already noted in the introduction when discussing the magnetization. The limaçon maps onto a pair of overlapping circles in the complex c plane, which is probably a more familiar presentation.

In contrast only two phases are present in the diagram for the Ising model on planar ϕ^4 graphs in the u plane, since there is no antiferromagnetic phase in this case (the graphs are not loosely packed - both odd and even loops can be present). The locus of Fisher zeroes in the u plane for the Ising model on planar ϕ^4 graphs is shown in Fig. 3. The interior of the loop is the ferromagnetic phase and the exterior the paramagnetic, with the physical transition lying at $u = 1/16$. The cusp point at $-\frac{1}{4}(\frac{49}{4} + 5\sqrt{6}) = -6.124362\dots$ does *not* represent an unphysical phase transition point, unlike the multiple point on the limaçon. as can be confirmed by looking at the discriminant $\Delta(g')$ of $cg'(z)(1-z)^3/(1-c^2)^2$. This will show up any non-generic points where multiple roots exist giving phase transition points as opposed to the generic first-order boundaries ⁴. The discriminant is proportional to

$$\Delta(g') \propto \frac{u^7(1-16u)^2}{(1-u)^{16}} \quad (29)$$

so the only place where non-generic behaviour appears apart from the trivial point, $u = 0$, is at the transition point $u = 1/16$. At this point the KPZ/DDK exponents $\alpha = -1$, $\beta = 1/2$, $\gamma = 2$ are manifested rather than the flat lattice Onsager exponents. In addition to the plotted curve a cut runs down the negative u axis from the cusp to $u = -\infty$. In this respect the locus of zeroes is more similar to that of the Ising model on a regular triangular lattice rather than the square lattice [9]. Obtaining zeroes for finite size graphs from the series expansion one also finds zeroes lying along the negative u axis.

Back in the complex $c = \exp(-2\beta)$ plane one has the locus shown in Fig. 4 with a physical transition point at $c = 1/4$ and a mirror image at $c = -1/4$, both with KPZ/DDK exponents. We have again omitted the cuts running up and down the imaginary axis from the cusp points at $\pm \frac{I}{2}(\frac{5}{2} + \sqrt{6}) = \pm I 2.474744872\dots$ to $\pm I\infty$ for clarity. In the c variable it is clear that these cuts, and the associated zeroes, appear because of the \sqrt{c} terms in the paramagnetic solutions g_{H_i} in equ.(8). Due to the cut on the imaginary axis the entire left hand region of the c plane exterior to the locus plotted in Fig. 4 forms an unphysical phase (labelled “O” in the parlance of [9]), whereas the exterior right hand region forms the (complex extended) paramagnetic phase. The O phase vanishes in the u plane since the sections of the cut on the imaginary axis in the c plane are folded onto the negative u axis. Nonetheless the presence of the cut means that it is not possible to make a circuit of the origin in the u plane in the paramagnetic region.

We have also plotted the numerically determined roots obtained from the coefficient of \tilde{g}^{79} in the expansion of $\log(\tilde{z}(\tilde{g})/\tilde{g})$ in Figs. 3,4. It is clear that the agreement with the analytically derived locus is very good for the roots closest to the critical point(s). The finite-size effects, which we have not investigated in detail, would be interesting to explore further since it can be seen that in the u plane the roots initially lie outside the analytic locus before moving inside it as the cusp is approached.

The Fisher zero locus on ϕ^4 graphs is thus, if anything, simpler than the square lattice locus – the antiferromagnetic phase is absent and there are no unphysical transition points such as the $u = -1$ point on the square lattice. The topology is closer to the locus of zeroes observed for regular triangular lattices which are also not self-dual, though the cut(s) do not extend into the ferromagnetic region as they do on the triangular lattice.

⁴The factor of $c/(1-c^2)^2$ has been included to match with the factors in the free energy in equ.(9) and the $(1-z)^3$ cancels the (irrelevant) denominator of $g'(z)$.

5 Dual Quadrangulations

Although the Ising model on planar ϕ^4 graphs does not display an antiferromagnetic transition it does on their dual random quadrangulations [17]. Again it is useful for orientational purposes to look at the locus of zeroes for the square lattice Ising model which corresponds to the case of regular quadrangulations. This gives the overlapping circles shown in Fig. 5.

The locus of zeroes for the random quadrangulations can formally be obtained by mapping the locus of Fig. 4 in the c plane to the c^* plane.

$$c^* = \frac{(1-c)}{(1+c)}, \quad (30)$$

which may also be written as $c^* = \tanh(\beta)$. The identification of the phases is, however, different for the dualized ϕ^4 diagram and the quadrangulations. In Fig. 6 we can see that this gives a ferromagnetic phase around the origin, a crescent shaped paramagnetic phase and an exterior region forming the antiferromagnetic phase. The boundaries of the crescent are inverse to each other in the unit circle, a section of which also forms the image of the cut along the imaginary axis in Fig. 4 and joins the horns of the crescent to $c = -1$ to form the *FM/AFM* boundary. These horns lie at $-0.719\,273\,115\,4... \pm I\,0.694\,727\,418\,2...$ and just as for the cusp point(s) in the u and c planes there is no sign of non-generic behaviour there. The numerically determined roots have again been plotted for comparison.

One can also obtain the locus for the quadrangulations directly by using the dualized expressions for g , replacing $c \rightarrow (1-c)/(1+c)$,

$$\begin{aligned} \tilde{g}_L &= \frac{1}{36} \frac{5c^2 - 22c + 5}{(1+c)^2}, \\ \tilde{g}_{H_{1,2}} &= -\frac{4}{9} \frac{2c^2 - c - 1 \pm (1+c)\sqrt{1-c^2}}{(1+c)^2}, \\ \tilde{g}_{H_{3,4}} &= \frac{4}{9} \frac{c^2 + c - 2 \pm (1+c)\sqrt{c^2-1}}{(1+c)^2}, \end{aligned} \quad (31)$$

and plotting $|\tilde{g}_L(c)| = |\tilde{g}_H(c)|$. The results are identical whichever method is used. The $\tilde{g}_L(c)$ is now appropriate for the paramagnetic phase in Fig. 6, and the $\tilde{g}_H(c)$'s cover the ferromagnetic and antiferromagnetic phases.

The dual quadrangulations display a ferromagnetic transition at $c = 3/5$ (the image of $c = 1/4$) and an antiferromagnetic transition at $c = 5/3$ (the image of $c = -1/4$), both with KPZ/DDK exponents. Looking at the dualized discriminant (c.f equ.(29)),

$$\tilde{\Delta} \propto \frac{(3c-5)^2(5c-3)^2(1+c)^{14}(1-c)^{14}}{c^{16}}, \quad (32)$$

we can see that this also vanishes at $c = -1$ as well as the transition points at $3/5, 5/3$. It would be an interesting exercise to determine the associated exponents in full from the matrix model formulation or series expansions, but we do not pursue this further here.

6 Discussion and Desiderata

We have seen that it is possible to obtain the locus of Fisher zeroes for the Ising model on both planar ϕ^4 graphs and their dual random quadrangulations by simply matching the moduli of the critical couplings $g(c)$ or $\tilde{g}(c)$ for the various phases. This gives the loci in Figs. 3/4 and 6 respectively which form an interesting contrast to their square lattice counterparts in Figs. 2 and 5. In particular, the lack of self-duality on the ϕ^4 graphs makes for less structure than on square lattices since there is no antiferromagnetic transition and the general picture is more similar to the loci seen for regular triangular lattices and the dual honeycomb lattice [9].

Although the considerations of [15] were for first-order transitions the fact that the phase boundaries of the complex extended phases generically display first-order behaviour means that the idea of matching

up the real part of different branches of the free energy also applies to the models here. The more general approach of [12, 14] and the idea of regarding the loci of zeroes as Stokes lines or complex phase boundaries also suggests that this will determine the loci correctly. Comparison with series expansions results, both from [5] and the much longer self-generated series here, found good agreement with the analytically determined loci. We saw that generating such series expansions to obtain either the Fisher or Lee-Yang zeroes for the Ising model on planar graphs reduced to the reversion of a series for $g(z)$ and taking a logarithm, both simple operations, and relatively long series could be produced without undue effort.

It is perhaps worth noting that various properties of Fisher zero loci discussed in [10] which were derived from general considerations still apply to the models considered here. We have:

- The loci of points where the free energy is non-analytic is symmetric about the $\Re c$ axis (“*Theorem 1*” of [10]) – applies to both ϕ^4 graphs and quadrangulations.
- If the graph has even co-ordination number the locus of zeroes is invariant under $c \rightarrow -c$ (“*Theorem 2*” of [10]) – applies to the ϕ^4 graphs.
- If the graph is bipartite the locus of zeroes is invariant under $c \rightarrow 1/c$ (“*Theorem 3*” of [10]) – applies to the random quadrangulations.

We have looked only cursorily at Lee-Yang zeroes in this paper, for which a circle theorem in the complex $y = \exp(-2h)$ plane still appears to be valid on both planar [5] and thin graphs [18]. We noted that the results for the series expansions still hold when $h \neq 0$, and a series in y to obtain the Lee-Yang zeroes could still be generated by reversion of $g(z)$. Since the form of \mathcal{Z} is identical for ϕ^3 planar graphs, an investigation of Fisher zeroes on planar ϕ^3 graphs and their dual triangulations along the lines of the work here would thus be perfectly feasible. This would make for an interesting comparison with other regular lattices and the cases discussed here since, as we have seen, the structure of the loci of Fisher zeroes is highly non-universal even when the phase transition in the Ising model is universal.

Finally, we note that similar methods to those employed here may be used to obtain the locus of Fisher zeroes for the (mean field) Ising and Potts model on thin random graphs [19].

7 Acknowledgements

W.J. and D.J. were partially supported by ARC grant 313-ARC-XII-98/41 and the EC IHP network “Discrete Random Geometries: From Solid State Physics to Quantum Gravity” *HPRN-CT-1999-000161*. We would like to thank Chris Eilbeck for useful discussions on numerical methods and Przemek Repetowicz for his expertise on series expansions.

8 Appendix A

The polynomial in u which appears as the coefficient of \tilde{g}^{79} in the expansion of $\log(\tilde{z}(\tilde{g})/\tilde{g})$. This was used to determine the zeroes plotted in Fig. 3 for comparison with the analytically determined limiting locus.

```

- 37139835653499716006137093004620701844717837598860560 u78
- 148105411685025580921368944483948303066640247852769586720 u77
- 219796631965060385324004998785213226455149375358517795237040 u76
- 164831966491059030819403027184073178546645417896670585118583360 u75
- 73190682361368063761602209974275459964883309418605799340499616080 u74
- 21193244550424189508255837901963813871588047644811792548846191056480 u73
- 4271156254827515627988674042672332480042287504111958952442525040283760 u72
- 627862147390520641370446437291183350790480810579190731147022437119076480 u71
- 69745140248196358151864786123993807529941628810020280214779959586962178000 u70
- 6018464875673457244143786208765208352061116125920486582535296176941628552480 u69
- 412471197424814031713421607686052888384939032979910093299169932719217502605680 u68
- 22861804785909511304850003848078876423860505468001445816621100351727090582759360 u67
- 1040388001009525627004038511792853014499415633466242701751022788738614223781869200 u66
- 3937229409789412050834300775784434139478345858309842059514852058286335631694924640 u65
- 125266997969827761711210438283071490296757418502909447129580208467158633229292650800 u64
- 33824235941762809316986439403557899119830643621806795895083691041491223423768922205440 u63
- 781506993375339419627869035781247001736394777182618059097298519992567856933676156704880 u62
- 15562658373901209414212760616146627814737888000032257222965672288658120697186968782275040 u61
- 268811911671136955690918042236856880858371066215093407241731389769889134493580751112933200 u60
- 4050291100241419582412182577585709209008056613597679444354569945583790578947675200406223040 u59
- 53504781415966480294594562472712153356937322011357889872884583481047270602536642303088638640 u58
- 622495367645869004219933292061848993497857662753083300275019010292939581507824341349692997280 u57
- 6404543438655411633219849404298860613153085517505116213303372819518740708536174835590579287440 u56
- 58485418180717913864496799218932794580143995855302867606977886170575639976699851845262721795200 u55
- 475621336785144578141093749216959112700270248123937785852140476541108616686976720192921759659120 u54
- 3454949138847954145125771003347606489152711556862180385372143917784666252021530028539664893182560 u53
- 22479199511986118388889724740161629827026678535630939603915122091636882657168104303228159674782800 u52
- 131329868076867196195186585236624456481415618356382317417014696466013312429780652860135768267296320 u51
- 690521599841649282635736801910885058607271123389022410819911445499545307915907348287733164897752240 u50
- 3274325328024256449458979614797082828181193217762090705841294573764309335044774708753150018652173600 u49
- 14028681139432688233381147758023731741378398828505334676962034681706261933990437547881433240006857360 u48
- 5440123137635701850404538743157365408447588153396502111539531577783242990447085082088897334313973760 u47
- 191239041521657795885877250378350106358177226586893476004928070338801521234269414232669291252489401040 u46
- 610291336906248150439271697453406834444702936621298381611047533416154600700953132073526490390632405920 u45
- 1770312091536857444373426280129531056383823804457933663200346345833395486708265307228705128695195679600 u44
- 4673258693673369170099996712465402139410313870189955652194788714038526152805740081647593630983237053760 u43
- 11238340128289348531242087550331250364185389607406579052122781101900272991182180944775170566681819386000 u42
- 24643620807293562049016307383826254746709674468010311230815770648930276238060169036875457070893380721120 u41
- 49316215047681422820639798034968563472661586153859146452324880638936874014462917442830512251412077320240 u40
- 9013183932281810459733336569785500994891715222936638893065298017192961284637989321929824868625942600320 u39
- 150539307460569060574873043134235781924850278322933804772229480942138558944046423812994722573756085825360 u38
- 229903670914274936494547986274227024806559809186604659564439155029892404257079655480106334324463382885920 u37
- 321195929010989242053422405330257454914814399821523791435254317299861335551419026344418606382633018360560 u36
- 410667245136280380010581522457335103688614698402729092669357283369677965166842035371819832521182880164800 u35
- 48066088461129261090046578897918281023736776948675848258097150679019327475680002989335685501198986450960 u34
- 515127622604009076515382991320921882654805662970841545228975271887370157242400946254339190729371860734560 u33
- 505572539992143017713391549930170518971477525159833401616072175808615633494794516723314803372928619903920 u32
- 45444054398009972288378100957933438165258237407744106629390938799888591553099389645099988347996759394560 u31
- 374106736311266598660706201323205892577430894328276767390142693909422925642543062380498942843073828251600 u30
- 282037307392349122318096395401444739778301936284237145311149810212523353375933495463993869693601796997280 u29
- 194690973545520420014650890857022846138498239021284276872938877733302758744011263203822896548354353908080 u28
- 123031667663724163290143244836151984882257781474006660444783619429304123640439106921897101552503284604480 u27
- 71152689559788776900734692668351990631384530566734957851066183734605762285678691522899649638001404881040 u26
- 37645077644878972338954061259578470473781833988432377397016223534337576278963315955825141659844837247200 u25

```

— 18212688770152920372331067819857158399286416752811996600134670652194813938813678169137029311984688169520 u^{24}
 — 8053088045624594957085039163949872370388432536121810011655001167011932667983907251509818773391710450560 u^{23}
 — 3252470645082229356008650751768353156845940016343565742435144703608857453346650919121596251905872636880 u^{22}
 — 1199037878489113778438716271817391517512781176088717654560134880626972165041017913820459566740270632480 u^{21}
 — 403173861504807914325983089651615786813837710424803782422307586554827984880680408117617036296222317680 u^{20}
 — 123545737931826333990589263018372737196158771136705218308890409337157363897683254886286406051621360320 u^{19}
 — 3446980603956652112712649188590819543046099324436123158311930137387052183055924535551928957561135760 u^{18}
 — 8747581221336382206763336472263174629514640810049804874785909198519454278642989719373646252543135840 u^{17}
 — 2016966904073261456791906783288877971694018387744544285386966376644936811743262591541510272304280880 u^{16}
 — 422040110288334497759627356286465867221287602590081491468592540570383771671547293848313282795512320 u^{15}
 — 80036988814102662395545702571530110662277119050351283201390143378307254063442392356336074807002080 u^{14}
 — 13737160482867657888903979612359904387039625719432395863706607709157730140315331444552427440036800 u^{13}
 — 2130581489746179897063191453661629432483663971225284474690803480225230394996040706276753337037600 u^{12}
 — 298084582170998682522557843634130692118118248948169065379102074737434795961756416684382725001600 u^{11}
 — 3754496621550752332227694572841010043722835844974349906421354497206822261619859885610212620000 u^{10}
 — 4247074844108597663669728712049132720278802778418177142466258256291478726641887125832109121600 u^9
 — 430155384350934174771440197370772245548350430019275647467244387233120149574187173959697949600 u^8
 — 38846640456271627441559966602880555242219998526979599170425784619478931564006336448368211200 u^7
 — 3109241968691735189036674456756079403285981061864652920257364770194926524810059222607549600 u^6
 — 218519863192071952043562258682613228805967293880235742328799873278069522182085472663592000 u^5
 — 13283468415320811624119223651865154826538028015964121931579143066280124387044588883314400 u^4
 — 680683119521593923666628073413708550282239032204436877326746488850479986486890462153600 u^3
 — 28058580972988347971863829784009239496026729839677340527392289791671643157102437191200 u^2
 — 845523959563531370690705608441021047213998439259969130238386790640994054828513707200 u
 — 1140887404597421591776554792039966147370831359556572145202708266673791740119521072800/79

References

- [1] V.A. Kazakov, Phys. Lett. **A119** (1986) 140.
- [2] D.V. Boulatov and V.A. Kazakov, Phys. Lett. **B186** (1987) 379.
- [3] M.L. Mehta, Comm. Math. Phys. **79** (1981) 327;
S. Chadha, G. Mahoux, and M. L. Mehta, J. Phys. **A14** (1981) 579.
- [4] V.G. Knizhnik, A.M. Polyakov, and A.B. Zamolodchikov, Mod. Phys. Lett. **A3** (1988) 819;
F. David, Mod. Phys. Lett. **A3** (1988) 1651;
J. Distler and H. Kawai, Nucl. Phys. **B321** (1989) 509.
- [5] J. Ambjorn, K. Anagnostopoulos, and U. Magnea, Mod. Phys. Lett. **A12** (1997) 1605;
Nucl. Phys. (Proc.Suppl.) **63** (1998) 751.
- [6] T.D. Lee and C.N. Yang, Phys. Rev. **87** (1952) 410.
- [7] C.N. Yang and T.D. Lee, Phys. Rev. **87** (1952) 404.
- [8] J. Lebowitz and O. Penrose, Comm. Math. Phys. **11** (1968) 99;
G. Baker, Phys. Rev. Lett. **20** (1968) 990;
R. Abe, Prog. Theor. Phys. **37** (1967) 1070; *ibid.* **38** (1967) 72; *ibid.* **38** (1967) 568;
S. Ono, Y. Karaki, M. Suzuki, and C. Kawabata, J. Phys. Soc. Japan **25** (1968) 54;
D. Gaunt and G. Baker, Phys. Rev. **B1** (1970) 1184;
P. Kortman and R. Griffiths, Phys. Rev. Lett. **27** (1971) 1439;
M. Fisher, Phys. Rev. Lett. **40** (1978) 1611;
D. Kurtze and M. Fisher, Phys. Rev. **B20** (1979) 2785;
M. Fisher, in: *Lectures in Theoretical Physics VII C* (University of Colorado Press, Boulder, 1965).
- [9] V. Matveev and R. Shrock, J. Phys. **A28** (1995) 1557; J. Phys. **A29** (1996) 803; J. Phys. **A28** (1995) 4859; J. Phys. **A28** (1995) L533-L539; Phys. Lett. **A204** (1995) 353; Phys. Rev. **E53** (1996) 254; Phys. Lett. **A215** (1996) 271; Phys. Rev. **E54** (1996) 6174.
- [10] V. Matveev and R. Shrock, J. Phys. **A28** (1995) 5235.
- [11] P. Repetowicz, U. Grimm, and M. Schreiber, Mat. Sci. Eng. **A294-296** (2000) 638.
- [12] C. Itzykson, R. Pearson, and J. Zuber, Nucl. Phys. **B220** [FS8] (1983) 415.
- [13] M. Staudacher, Nucl. Phys. **B336** (1990) 349.
- [14] G. Marchesini and R. Shrock, Nucl. Phys. **B318** (1989) 541.
- [15] M. Biskup, C. Borgs, J.T. Chayes, L.J. Kleinwaks, and R. Kotecky, Phys. Rev. Lett. **84** (2000) 4794;
and preprint “Partition function zeros at first-order phase transitions”.
- [16] J. von zur Gathen and J. Gerhard, *Modern Computer Algebra* (Cambridge University Press, Cambridge, 1999).
- [17] C. Baillie and D. Johnston, Phys. Lett. **B357** (1995) 287.
- [18] L.C. de Albuquerque, N.A. Alves, and D. Dalmazi, Nucl. Phys. **B580** (2000) 739.
- [19] B.P. Dolan, W. Janke, D.A. Johnston, and M. Stathakopoulos, “Thin Fisher Zeroes” [**cond-mat/0105317**].

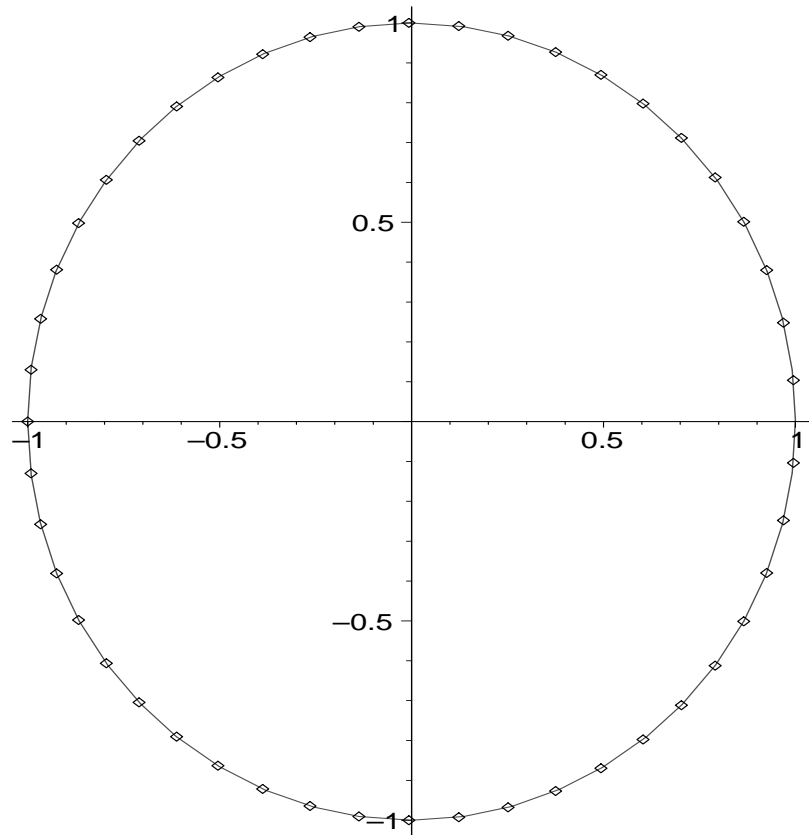


Figure 1: Lee-Yang zeroes in the complex $y = \exp(-2h)$ plane for the Ising model on planar ϕ^4 graphs calculated from an expansion of $\tilde{z}(\tilde{g})/\tilde{g}$ to order y^{31} . They clearly lie on the unit circle.

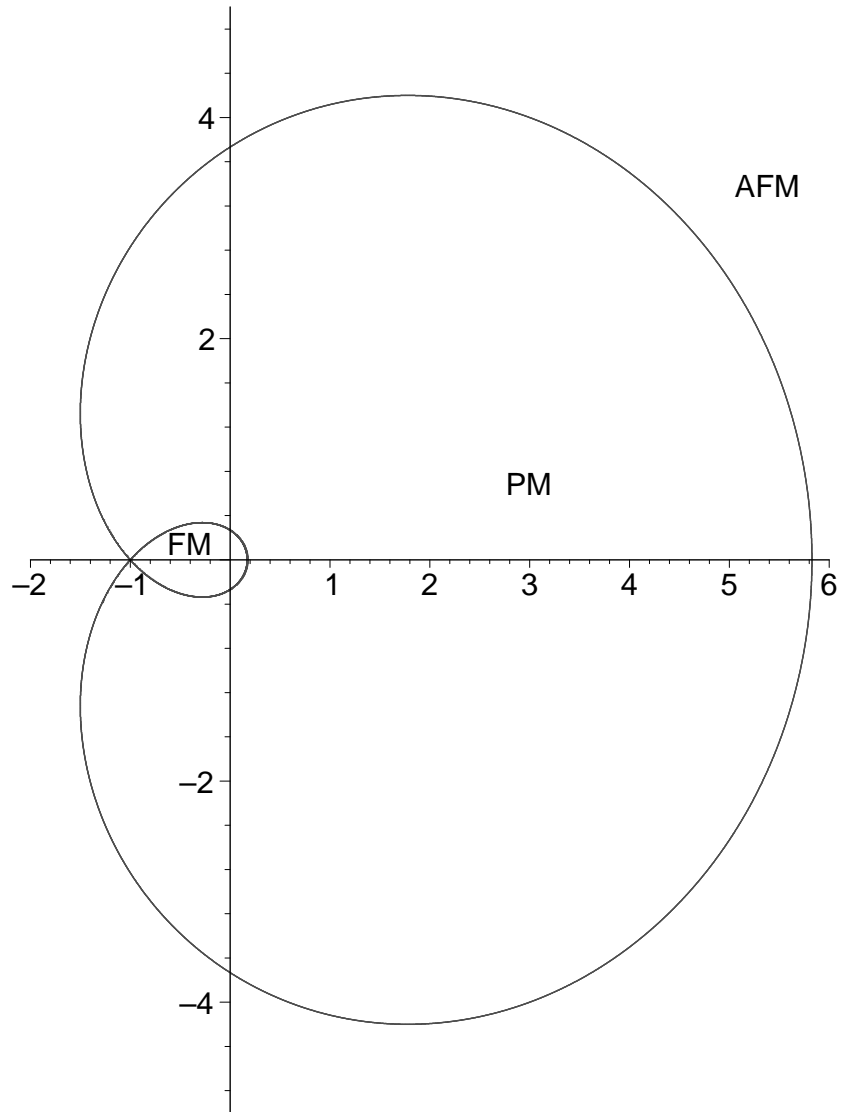


Figure 2: The locus of Fisher zeroes in the complex $u = \exp(-4\beta)$ plane for the Ising model on the square lattice. The ferromagnetic phase lies inside the inner loop, the paramagnetic phase between the loops and the antiferromagnetic phase in the exterior.

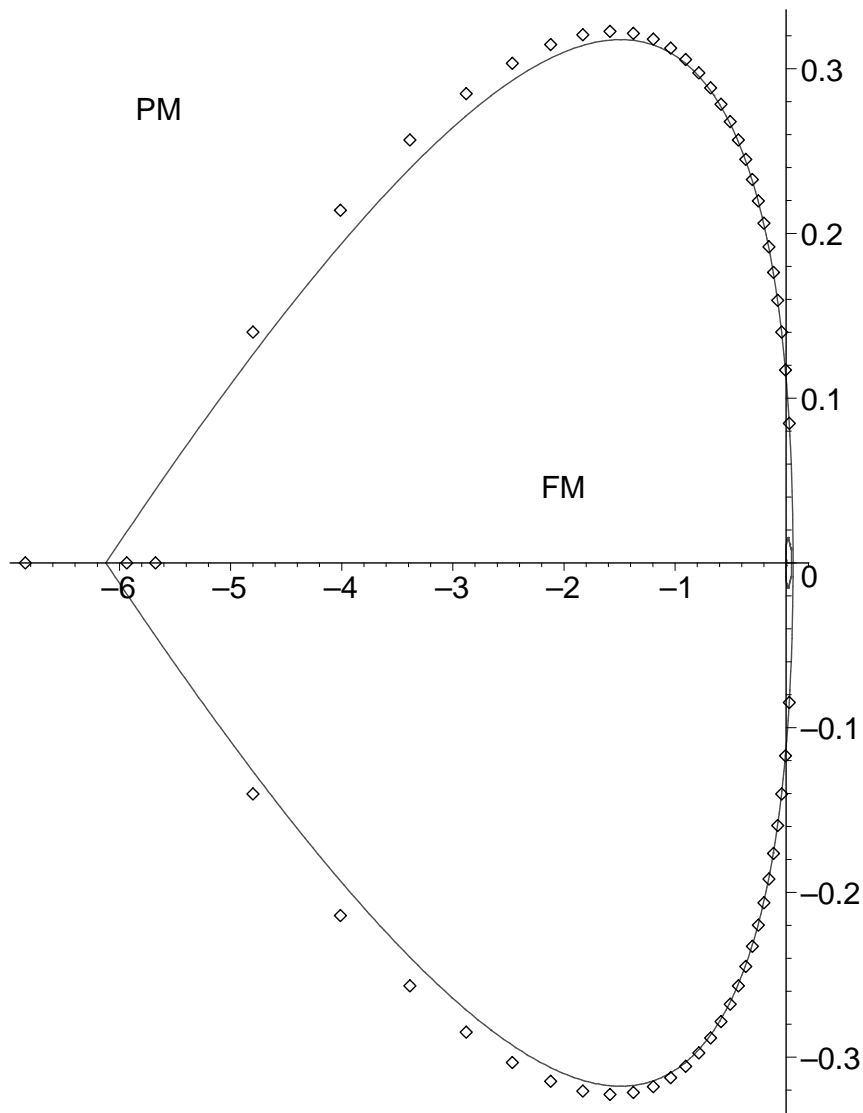


Figure 3: The locus of Fisher zeroes in the complex $u = \exp(-4\beta)$ plane for the Ising model on planar ϕ^4 graphs. Some of the zeroes calculated from the series expansion to order g^{79} in Appendix A are also plotted for comparison, though we have not plotted the zeroes lying at large negative u values on the axis.

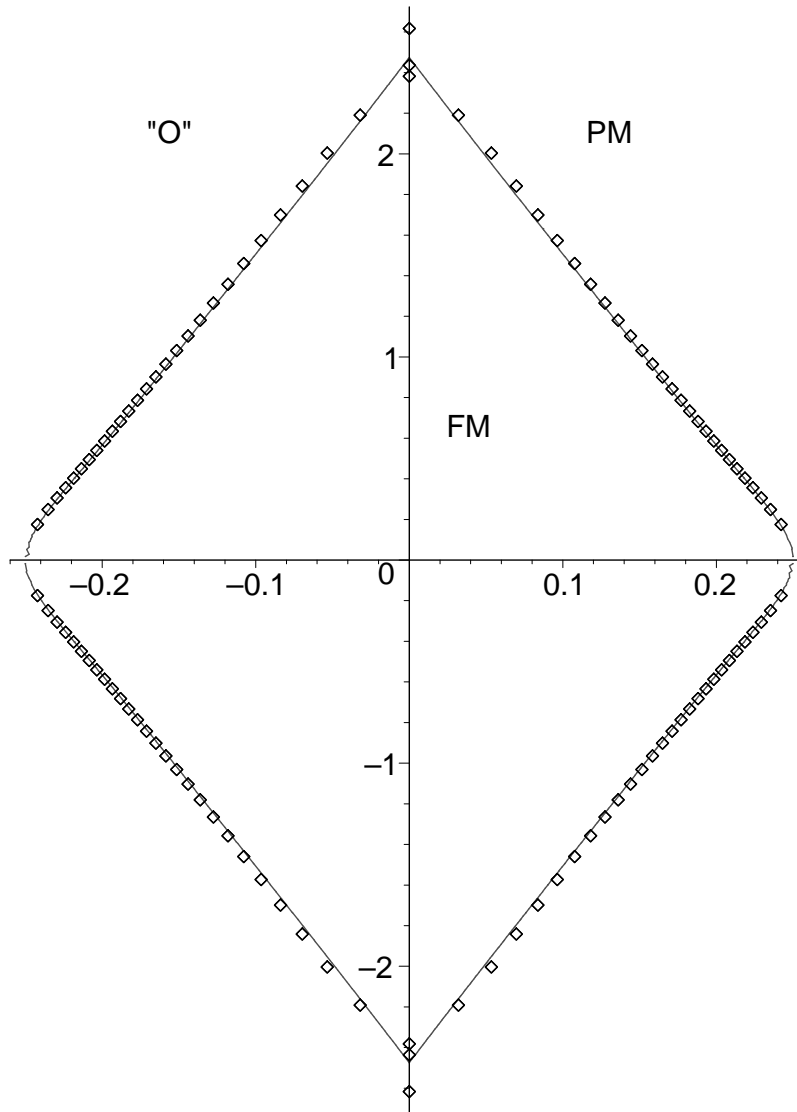


Figure 4: The locus of Fisher zeroes in the complex $c = \exp(-2\beta)$ plane for the Ising model on planar ϕ^4 graphs. The interior of the curve is the ferromagnetic FM region and the exterior the paramagnetic PM and unphysical O phases, separated by the cuts on the imaginary axis which we have not plotted.

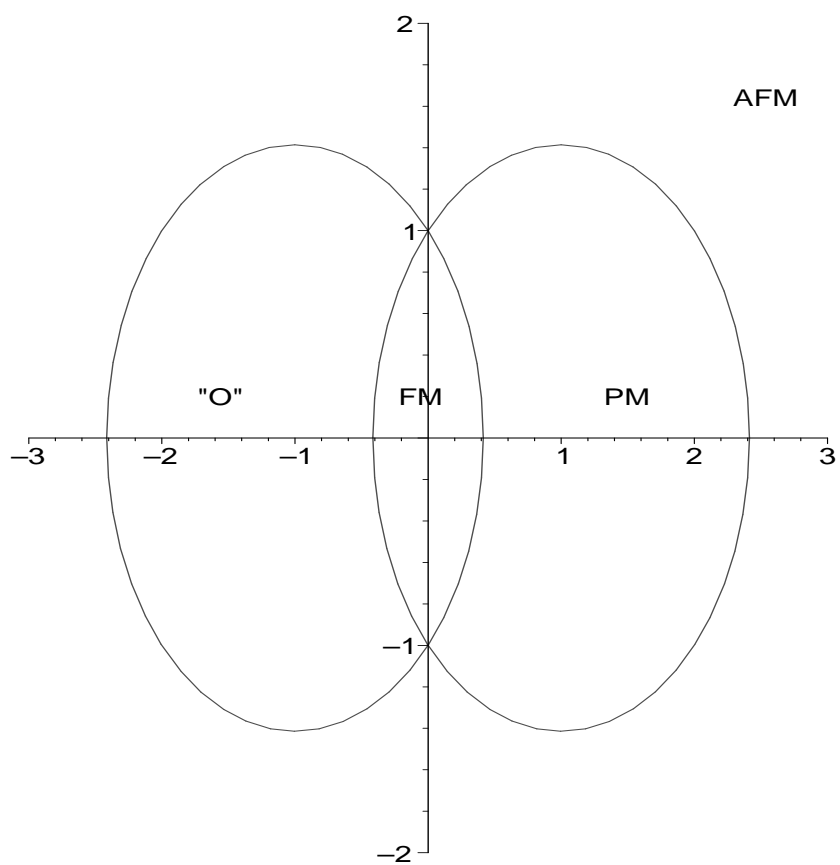


Figure 5: The locus of Fisher zeroes in the complex c plane for the Ising model on the square lattice. The O region is not connected to any physical values of c .

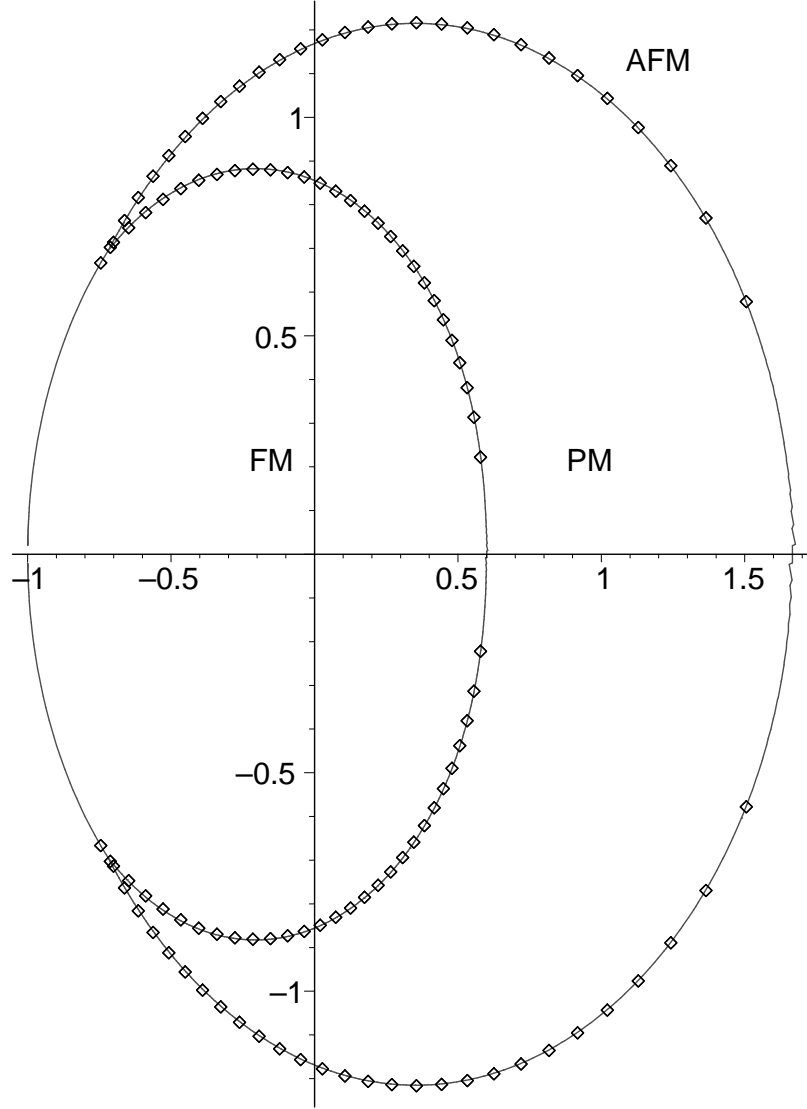


Figure 6: The locus of Fisher zeroes in the complex c plane for the Ising model on random quadrangulations. This is formally identical to the mapping of the locus in Fig. 5 into the $c^* = (1-c)/(1+c) = \tanh(\beta)$ plane but the identification of the phases is different. For quadrangulations the interior of the crescent is the paramagnetic (PM) phase and the two horns of the crescent are joined to $c = -1$ by arcs of the unit circle which are the images of the imaginary axis cuts in Fig. 4. These form the boundary between the inner FM and exterior AFM phases.